Multi-mass velocity map imaging study of the ultraviolet photodissociation of dimethyl sulfide using single photon ionization and a PImMS2 sensor

Matthew Bain,[1] Christopher S. Hansen,[2, a)] and Michael N. R. Ashfold[1, b)]
[1)] *School of Chemistry, University of Bristol, Cantock's Close, Bristol, BS8 1TS, UK*
[2)] *School of Chemistry, University of New South Wales, Sydney, NSW 2052, Australia*

(Dated: 20 August 2018)

This study of the photodissociation of dimethyl sulfide at $\lambda = 227.5$ nm demonstrates the opportunities (and some of the challenges) of product detection using vacuum ultraviolet photoionization combined with recently developed multi-mass imaging methods. The capability of imaging different charged products simultaneously allows determination of the primary fragmentation dynamics through, for example, product fragment momentum and angular distribution matching, and reveals potential complications from dissociative ionization, product alignment-dependent photoionization probabilities, and the effects of space charging.

Keywords: multi-mass imaging; single photon ionization; photodissociation; dimethyl sulfide

Velocity map imaging (VMI) methods find widespread use as a means of determining the velocity distributions of atoms or small molecular fragments formed in gas phase photodissociation processes or as products in bimolecular scattering events.[1–3] Typically, one (or more) of the neutral photoproducts or scattering products of interest are ionized at their point of creation, using visible or ultraviolet (UV) photons from a pulsed laser and an appropriate resonance enhanced multiphoton ionization (REMPI) scheme.[3] The resulting ions are accelerated by voltages applied to a suitably designed set of ion optics, enter a field free drift region and ultimately impinge on a 2-D position sensitive detector. The detector in most VMI experiments is a stack of microchannel plates (MCPs), which convert each incident ion into a cloud of electrons without any significant loss of spatial resolution. The electrons exiting the rear face of the MCP stack are accelerated onto a phosphor screen and the resulting spots of emission are recorded using a charge coupled device (CCD) camera. The ion masses are confirmed by their measured times of flight (ToFs) to the detector and their velocity (*i.e* speed and angular) distributions are revealed by analyzing the pattern of ion impacts on the detector. The photoelectron is light enough that its release (upon ionization) typically imparts little recoil on the partner ion, and the derived ion velocities thus provide a reliable measure of the velocities of the neutral product of interest.[4] The velocity distribution of the partner product can usually be inferred by energy and momentum conservation arguments.

REMPI detection methods offer several advantages. In the case of atoms and small, light (typically diatomic) fragments, the choice of probe wavelength will usually establish not just the mass (and thus the identity) of the probed species, but also its quantum state. This specificity can lead to very 'clean' ion TOF spectra. In many cases, only the target fragment will be ionized when exciting at the chosen REMPI wavelength. In the event of contamination from unintended ionization events yielding ions with other masses, these can be rejected by time-gating the MCPs so that the detection sensitivity is high only for the brief period corresponding to the ion TOF of interest. However, this approach has its limitations. Principal amongst these is that REMPI is far from universally applicable – the number of species which are larger than diatomics for which there exists a well characterised REMPI scheme is small – and only one product species (and often only one quantum state of that species) is ionized and thus imaged in an experiment.

The present study demonstrates a way of overcoming these limitations. Replacing the visible or UV REMPI probe photons with a sufficiently short wavelength vacuum UV (VUV) photon enables ionization with a single photon, allowing detection of many more species.[5–10] Single photon ionization (SPI), sometimes termed 'universal' ionization, predates the VMI technique and is a recognised alternative to REMPI as a detection method. SPI is far more general – any species with an ionization potential (IP) smaller than the VUV photon energy can be ionized – and thus offers a means of detecting multiple products simultaneously. However, SPI is rarely quantum state specific. In the context of VMI experiments this can actually be advantageous, when the product state information can be derived from the image itself, or when product yields are too low for quantum state specific product detection. In all cases, SPI offers an appealing increase in generality, but the read-out rate of traditional CCD cameras is too slow to allow time-gated imaging of more than one feature in the ion TOF spectrum. To exploit the benefits of SPI methods more fully it would be beneficial to image many different product ions at the same time – so called multi-mass imaging – which we achieve here through use of a CMOS-based Pixel Imaging Mass Spectrometry (PImMS2) sensor.[11] The spatial resolution of this sensor is 324 x 324 pixels,

[a)] Electronic mail: christopher.hansen@unsw.edu.au
[b)] Electronic mail: mike.ashfold@bristol.ac.uk

TABLE I. Ionization potentials (IPs) and enthalpies of formation of DMS and of selected fragment species (neutrals and cations – ΔfH(n) and ΔfH(c), respectively) relevant to the present work.

	IP / eV	ΔfH(n) / eV	ΔfH(c) / eV
CH3SCH3	8.6903 ± 0.0009[18]	-0.22[19]	8.42[19]
CH3S	9.262 ± 0.005[20]	1.346 ± 0.018[21]	10.62 ± 0.022[20]
CH3	9.843 ± 0.002[22]	1.552 ± 0.001[23]	11.392 ± 0.001[24]
HCS	7.499 ± 0.005[25]	3.11 ± 0.09[25]	10.52 ± 0.09[25]

each of which contains four memory registers capable of reporting ion events (*i.e.* their x,y coordinates) with a time (t) resolution as short as 12.5 ns.

$$CH_3SCH_3 \xrightarrow[\lambda = 227.5\ nm]{h\nu} CH_3 + SCH_3 \qquad (1)$$

Here we use the photodissociation of dimethyl sulfide (DMS) at a wavelength of λ = 227.5 nm, as shown in equation 1, to illustrate some of the opportunities but also some of the challenges afforded by combining SPI and multi-mass imaging methods in studies of molecular photodissociation dynamics. DMS photolysis at this and nearby UV wavelengths has been investigated previously by TOF-mass spectrometry and VMI methods following REMPI of the CH3 radical products. These prior studies reveal that the ground ($\tilde{X}$) state CH3 fragments are formed predominantly in their zero-point vibrational (v = 0) level.[12–14] The velocity distribution is anisotropic, and is consistent with prompt (*i.e.* sub 100 fs) C–S bond fission following parent excitation via a transition dipole moment ($\boldsymbol{\mu}$phot) that is aligned perpendicular to the plane defined by the C–S–C atoms.[15–17]

None of the prior studies monitored the CH3S partner fragment, but the derived CH3($\tilde{X}$, v = 0) speed distribution implied that of the energy available to the system (Eavl, defined as the difference between the photolysis photon energy and the CH3–SCH3 bond dissociation energy), 74 % is deposited into translational energy of the photofragments. As the CH3 fragment is measured to be internally 'cold', the remaining 26 % must be partitioned amongst the rotational and vibrational states of the partner CH3S.

As table I shows, the IPs of the parent molecule and both primary fragments in equation 1 lie below that of a 118.2 nm photon (Ephot = 10.48 eV) which can be conveniently generated by frequency tripling the third harmonic of a table-top Nd:YAG laser (λ = 355 nm). HCS^+ is a dissociative ionization product and will be discussed later.

The experimental apparatus and procedures have been detailed previously[26] and are only summarized briefly. DMS (Sigma–Aldrich, stated purity > 99 %) was seeded in helium (1 % mixture, 800 mbar backing pressure), expanded through a pulsed valve into the source vacuum chamber and skimmed *en route* to the differentially pumped interaction region bounded by the repeller and extractor electrodes of the ion optics assembly.[27] Here the molecular beam (which defines the z-direction) is intercepted by the counter–propagating (along the y–axis) photolysis and, t = 30 ns later, SPI laser pulses. The former (λ = 227.5 nm, 0.5 mJ pulse^{-1}) was generated by frequency doubling the output of a Nd:YAG pumped dye laser and focused into the interaction region using a lens with a focal length (f.l.) of 20 cm. The 118.2 nm photons were generated by focusing (f.l. = 30 cm) the third harmonic of a second Nd:YAG laser (λ = 355 nm, 13 mJ pulse^{-1}) into a cell containing a 1:12 phase matched mixture of xenon (N5.0 grade, BOC) and argon (N6.0 grade, BOC) at a total pressure of 300 mbar. This cell was coupled directly to the vacuum chamber with a custom lithium fluoride lens (f.l. = 14 cm at 118.2 nm) to direct the 118.2 nm photons into the interaction region.

Under standard operating conditions both the photolysis and SPI laser pulses were vertically linearly polarized (along x), but insertion of a double Fresnel rhomb allowed rotation of either polarization vector in the xz plane. Cations formed in the interaction region are accelerated along z and then enter a 46 cm field free drift region, separating in time according to their mass to charge (m/z) ratio before striking a triple stack MCP detector coupled to a P47 phosphor screen. The detector gain can be time–gated to allow selection of just a portion of the ion TOF spectrum and the screen is imaged by a PImMS2 sensor[11,28] through a Nikon NIKKOR 55 mm macro lens (f / 2.8). The time resolution of the PImMS2 sensor was set to 25 ns which, for the chosen ion optics voltages, provides 8–10 time slices through each of the m/z peaks of interest.

The data were processed by first centroiding the (x, y, t) event lists associated with each laser shot in space and time to reduce event clusters to single ion events using a previously described algorithm.[29] A TOF spectrum can be created at this stage by summing all events arriving in the various time bins and converted to a m/z spectrum by comparison with the TOFs of a known set of masses. Ion images, either a central slice or a crushed image, were constructed by plotting the (x, y) coordinates of events within, respectively, either the single time bin corresponding to the peak TOF signal or the full spread of TOFs associated with the appropriate m/z. The resulting ion images typically contained a few disproportionately intense pixels associated with dark counts on the sensor, which were 'trimmed' by scanning through the pixel array, identifying any pixel with an intensity more than twice the average of its eight immediate neighbours and resetting that intensity to the average value. The crushed images were then reconstructed using a polar onion peeling algorithm[30] and the recoil anisotropy parameter (β) of any feature of interest determined by fitting to equation 2, where $P2(\cos\theta)$ is the second order Legendre polynomial and θ the angle between the electric vector of the photolysis laser, $\boldsymbol{\epsilon}$phot, and the recoil velocity. Radius to velocity calibration was achieved

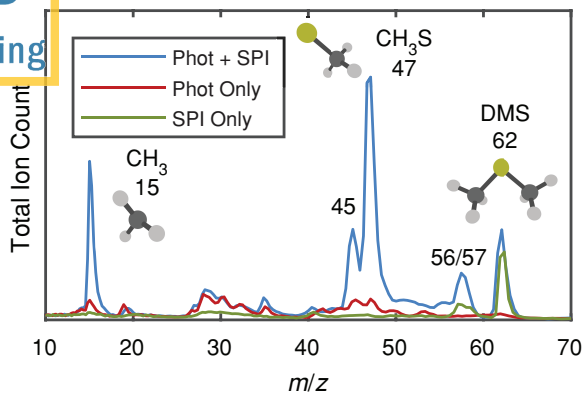

FIG. 1. Mass spectra derived from TOF spectra measured with the photolysis ($\lambda = 227.5$ nm) and SPI ($\lambda = 118.2$ nm) laser pulses present in blue and with one or other of these lasers blocked (red and green as indicated in the inset). The $\boldsymbol{\epsilon}$ vector in all cases was aligned along x, *i.e.* parallel to the front face of the detector, and the m/z scale has been derived from the measured TOFs assuming that the SPI laser pulse defines time zero. The most abundant ion under all conditions is the parent DMS^+ ion at m/z 62, but its detected signal is reduced by ensuring that the detector sensitivity is maximal only for arrival times corresponding to m/z 10–60.

by monitoring the known O^+ signals following photodissociation of O2 and subsequent REMPI of the O atom fragments at $\lambda = 225.67$ nm.[31]

$$I(\theta) \propto 1 + \beta P_2(\cos\theta) \quad (2)$$

Figure 1 shows the m/z spectrum obtained by $\lambda = 227.5$ nm photodissociation of DMS and subsequent $\lambda = 118.2$ nm SPI (in blue), together with the spectra obtained with only the 227.5 nm (red) or 118.2 nm (green) radiation present. Peaks in the two color spectrum that overlap substantially with either one color contribution (*e.g.* the parent ion peak at m/z 62) are not considered further. The two color spectrum is dominated by peaks at m/z 15 ($CH3^+$) and 47 ($CH3S^+$), with less intense peaks at m/z 45 and ~56/57. The former is attributable to HCS^+, a known unimolecular decay product from internally excited $CH3S^+$ ions.[32] As Table I shows, HCS^+ loss from $CH3S^+$ is essentially thermoneutral, though one theoretical study suggests a barrier of 1.39 eV in the elimination reaction coordinate.[33] The source of the small peak at m/z ~56/57 is less clear, but a similar feature was observed in a recent UV photolysis study of 2-bromothiophene and tentatively assigned to $HCCS^+$ and/or $H2CCS^+$ fragment ions.[26] These weaker peaks serve to illustrate the probability of dissociative ionization when using SPI methods to detect photofragments formed with a broad spread of internal energies.[9] However, as shown in the earlier 2-bromothiophene study[26] and below, access to the associated ion image will often suffice to identify and accommodate this complication.

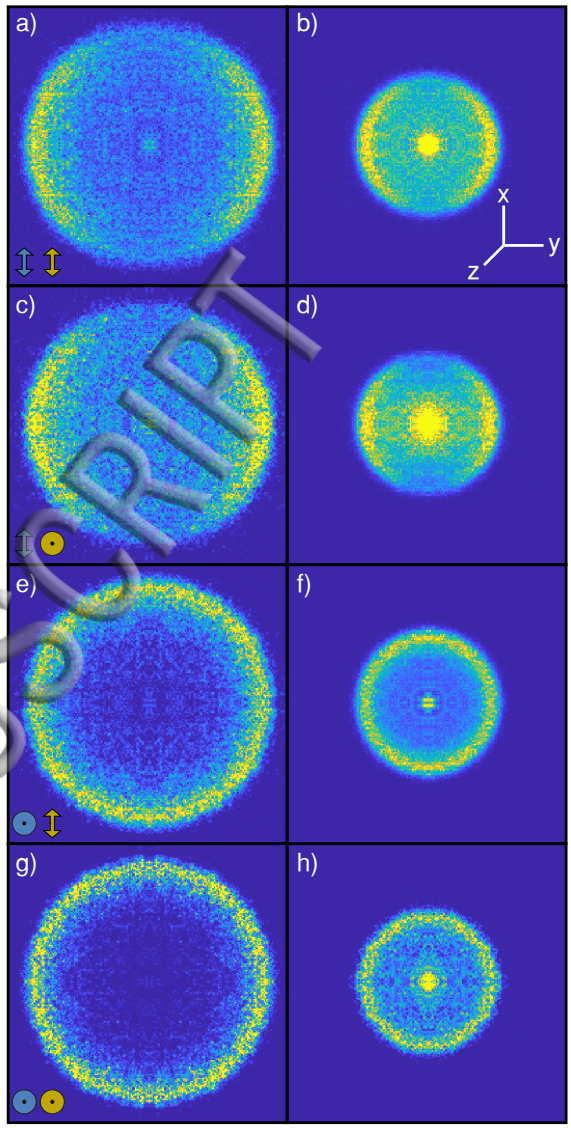

FIG. 2. Images of the m/z 15 ($CH3^+$) and 47 ($CH3S^+$) ion signals following $\lambda = 227.5$ nm photodissociation of DMS and subsequent SPI at $\lambda = 118.2$ nm (left and right hand columns, respectively). Each row shows the images recorded using different combinations of photolysis (blue) and probe (yellow) laser polarization vectors (along x, indicated by the double headed arrow, or z, shown by an annulus, in each of the left hand images). The central dot in each $CH3S^+$ image is from residual one color contributions; as this is radially distinct, no background subtraction was performed.

Figure 2 shows crushed ion images of the m/z 15 ($CH3^+$, left) and 47 ($CH3S^+$, right) ion signals for the various combinations of photolysis (blue) and probe (yellow) laser polarizations ($\boldsymbol{\epsilon}$phot and $\boldsymbol{\epsilon}$SPI, respectively), as indicated at the bottom left of each row. Images derived from just the central 25 ns slice of the associated TOF peaks are quantitatively similar. Illustrative slice images are shown in Figure S1 in the supplementary information

(SI). Crushed images of the m/z 45 and ~56/57 ion signals are shown in Figure S2. The $CH3^+$ image recorded with both ϵphot and ϵprobe parallel to x (figure 2 (a)) is the closest analogue to those reported previously using REMPI detection methods.[12,13,15–17] The best fit β parameter, –0.77 ± 0.03 (where the uncertainty represents a 95 % confidence interval) matches well with the literature values and with prior conclusions that dissociation is prompt and that $\boldsymbol{\mu}$phot at $\lambda = 227.5$ nm lies perpendicular to the C–S–C plane in the parent DMS. Momentum conservation would imply that the CH3 and CH3S fragments should display the same recoil anisotropy but, as figure 2 (b) shows, the $CH3S^+$ image appears noticeably less anisotropic; the best–fit anisotropy parameter is β = –0.50 ± 0.04. However, expectations based on momentum matching considerations are satisfied by the $CH3^+$ and $CH3S^+$ images recorded with ϵSPI aligned along z. The best–fit β values for the data shown in Figs. 2 (c) and 2 (d) are –0.77 ± 0.02 and –0.75 ± 0.03, respectively. Figures 2 (e–h) show the corresponding $CH3^+$ and $CH3S^+$ images recorded with ϵphot directed along the TOF axis (*i.e.* parallel to z). Perpendicular dissociation in this case should result in an equal probability of fragments recoiling in any direction within the xy plane and the measured images are reassuringly isotropic.

The sensitivity to probe laser polarization revealed by comparing figures 2 (b) and (d) is a classic signature of fragment alignment.[34–36] The ionization probability is proportional to $|\boldsymbol{\epsilon}_{\mathrm{SPI}}.\boldsymbol{\mu}_{\mathrm{ion}}|^2$, where $\boldsymbol{\mu}$ion is the transition dipole moment between the neutral species and the cationic continuum state. If $\boldsymbol{\mu}$ion has a preferred orientation in the frame of the fragment and the SPI transition is not saturated, then the SPI probability will be sensitive to any anisotropy in the distribution of these recoiling fragments. As noted previously, C–S bond fission in the parent DMS is initiated by photoexcitation via a transition with $\boldsymbol{\mu}$phot perpendicular to the plane containing the C–S–C backbone. Therefore the forces driving the prompt fission of the C–S bond (eq. 1), and the velocity vectors of the nascent CH3 and CH3S fragments, will be largely confined to that plane. Given the non–linear parent geometry, the latter are likely to be formed rotationally excited and, more importantly in the present context, to be rotating with their C–S bond confined to that plane (*i.e.* with their rotational angular momentum vector $\boldsymbol{J}$CH3S preferentially parallel to $\boldsymbol{\mu}$phot).

The inferred spatial alignment of the CH3S fragments was investigated further by recording images with ϵphot parallel to x and ϵSPI aligned at various angles ϕ in the xz plane (with $\phi = 0°$ defining the x axis) and fitting the returned angular distributions in terms of eq. 2. As figure 3 shows, the angular anisotropy parameter for the $CH3^+$ ions is insensitive to changes in ϕ, but the magnitude of the best fit β parameter for the $CH3S^+$ ions increases smoothly from ~ –0.5 when $\phi = 0°$ (as in figure 2 (b)) to ~ –0.75 when $\phi = 90°$ (figure 2 (d)). This evolution can be understood if $\boldsymbol{\mu}$ion for CH3S at λ = 118.2 nm is preferentially oriented along the C–S bond.

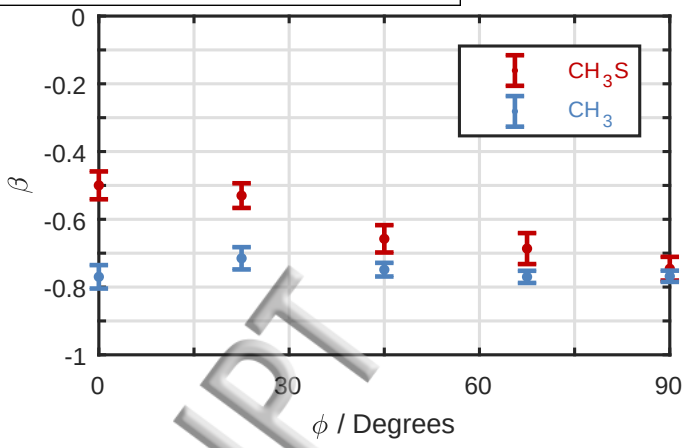

FIG. 3. β parameters derived by fitting reconstructed images of m/z 15 ($CH3^+$, blue) and 47 ($CH3S^+$, red) ion signals following $\lambda = 227.5$ nm photodissociation of DMS and subsequent SPI at $\lambda = 118.2$ nm measured with ϵphot parallel to x and ϵSPI aligned at various angles ϕ to the x axis. The displayed error bars represent 2σ (95 % confidence interval). Angular distributions and the best-fits for CH3 and CH3S data recorded at $\phi = 0°$ and 90° are shown in figure S3 of the SI.

These observations highlight another factor that requires recognition when using SPI methods; if the fragments are aligned, the SPI probability may well be sensitive to the VUV laser polarization.

Radial integration of the $CH3^+$ and $CH3S^+$ images in figures 2 (a) and (b) yields the respective speed, momentum and total kinetic energy (ET) distributions shown in figures 4 (a), (b) and (c). The ET distribution derived from the $CH3^+$ data matches that observed in the previous REMPI imaging studies of the CH3(v = 0) products, reinforcing the conclusion that the CH3 fragments from the UV photodissociation of DMS at $\lambda = 227.5$ nm are formed predominantly in their v = 0 level.[13] The neutral CH3 and CH3S products arise via a common dissociation process (eq. 1), so their respective momenta should match, and either speed distribution should return the same ET distribution. But this requirement only holds for the measured $CH3^+$ and $CH3S^+$ data if the ionization efficiencies of the neutral species are insensitive to the particular quantum states in which they are formed. The extent to which the respective momentum distributions match (figure 4 (b)) supports the validity of such an assumption in the present case. However, the ET distributions (figure 4 (c)) peak at a value (ET(peak)) below the maximum allowed by energy conservation (indicated by a vertical arrow in figure 4 (c) and calculated assuming $D0$(CH3S–CH3) = 3.13 ± 0.04 eV[37] and that the CH3 products are all in their v = 0 level). The present work implies a spread of internal energy in the CH3S products, with a most probable value $<E\mathrm{int}>$ ~0.7 eV. The agreement between the $CH3^+$- and $CH3S^+$- derived ET(peak) values in figure 4 (c) confirms that the ionization probability of CH3S at $\lambda = 118.2$ nm is indeed

rather insensitive to the initial quantum state. However, the observation of the m/z 45 HCS^+ fragment ions suggests that some CH3S fragments are formed with sufficient Eint to undergo dissociative ionization after SPI at $\lambda = 118.2$ nm. The momentum distribution (dashed curve in figure 4 (b)) derived from this HCS^+ image (see figure S2 of the SI) is sensibly consistent with a scenario wherein these fragment ions emerge with relatively little additional kinetic energy from an expanding Newton sphere of primary $CH3S^+$ ions.

Close inspection of figure 4 (b) shows that the momentum distribution of the $CH3S^+$ ions is marginally broader than that of the $CH3^+$ ions. This difference is more apparent in the corresponding ET plots, and would be further enhanced were we to include the HCS^+ fraction from the primary CH3S yield. This difference is also independent of either the photolysis or SPI laser polarization, and is most likely attributable to space charge effects. This is a third cautionary note illustrating some of the extra considerations required with SPI detection methods. The number and variety of ions formed when using SPI detection methods will generally be much higher than in most REMPI-based product imaging studies wherein only one species, and often just one quantum state of that species, is ionized. Well planned and executed REMPI-based studies offer the best opportunities for rigorously demonstrating product velocity distributions and the momentum matching of partner products, but such demonstrations would require viable REMPI schemes for both fragments, and a sequence of measurements probing successive quantum states of both species.

In summary, the photodissociation of dimethyl sulfide at $\lambda = 227.5$ nm has been investigated with VMI methods using VUV single photon ionization of the primary CH3 and CH3S photoproducts and a fast framing event-triggered PImMS2 sensor that allows simultaneous imaging of multiple fragment ions. The study confirms and extends existing knowledge concerning the UV photofragmentation dynamics of dimethyl sulfide and illustrates the broad applicability of SPI (*cf.* REMPI) based imaging methods, but also serves to illustrate some of the complexities that accompany SPI–based detection methods. Specifically, product quantum state specificity is foregone in exchange for universality and, as shown in this study, dissociative ionization, product alignment, and space charge effects may all need to be considered when interpreting measured images and the neutral photoproduct velocity information derived through their analysis.

Supplementary Material

See supplementary material for the following supporting information: Central slices of the VMI data presented in crushed form in Figure 2. Crushed images for the m/z 45 and 56/57 peaks. Angular plots of the $CH3^+$ and $CH3S^+$ ion signals from reconstructed images obtained with $\phi = 0°$ and 90°. Speed, momentum and ET spec-

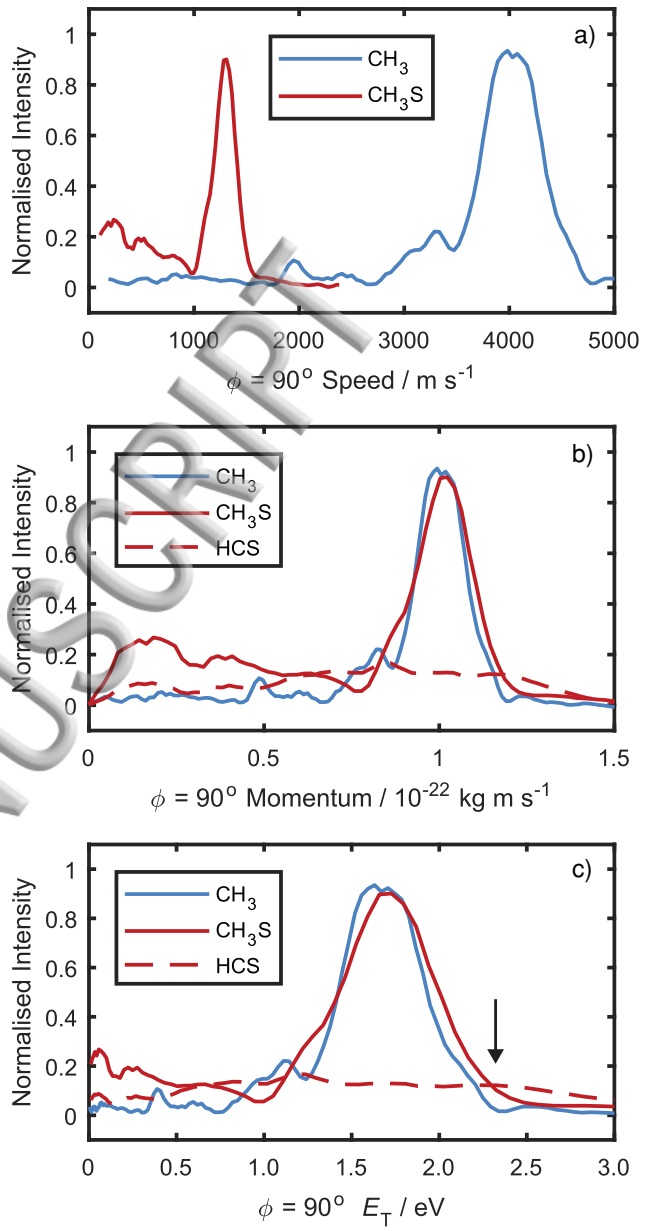

FIG. 4. (a) Normalized CH3 (blue) and CH3S (red) fragment speed distributions derived from the respective $CH3^+$ and $CH3S^+$ images following $\lambda = 227.5$ nm photolysis of DMS with ϵphot aligned parallel to x and ϵSPI aligned along the z axis ($\phi = 90°$). (b) Normalized momentum distributions derived from the CH3 and CH3S speed distributions (blue and red solid lines, respectively) along with the momentum distribution derived from analysis of the HCS^+ image (dashed red line). The area of the latter (relative to that of the CH3S distribution) has been scaled to match the ratio of the area beneath the m/z 45 and 47 peaks in figure 1. (c) ET distributions derived from the respective momentum distributions, with the vertical arrow indicating the maximum ET allowed by energy conservation. Equivalent data for $\phi = 0°$are shown in figure S4 of the SI.

tra analogous to those shown in figure 4 but with $\phi = 0°$.

Acknowledgements

Funding from the Engineering and Physical Sciences Research Council (EPSRC, Programme Grant EP/L001593) is gratefully acknowledged. The raw ion events data can be retrieved from the University of Bristol's research data repository and accessed using the following DOI: 10.5523/bris.2tvc0sfgngd752kwxbqltlgffv

[1]D. W. Chandler and P. L. Houston, J. Chem. Phys. **87**, 1445 (1987).
[2]A. T. J. B. Eppink and D. H. Parker, Rev. Sci. Instrum. **68**, 3477 (1997).
[3]M. N. R. Ashfold, N. H. Nahler, A. J. Orr-Ewing, O. P. J. Vieuxmaire, R. L. Toomes, T. N. Kitsopoulos, I. A. Garcia, D. A. Chestakov, S. M. Wu, and D. H. Parker, Phys. Chem. Chem. Phys. **8**, 26 (2005).
[4]D. H. Parker, R. F. Delmdahl, B. B. L. G. Bakker, and H. Loock, J. Chin. Chem. Soc. **48**, 327 (2013).
[5]N. P. Lockyer and J. C. Vickerman, Laser Chem. **17**, 139 (1997).
[6]S. H. Tsai, C. K. Lin, Y. T. Lee, and C. K. Ni, Rev. Sci. Instrum. **72**, 1963 (2001).
[7]C. K. Ni and Y. T. Lee, Int. Rev. Phys. Chem. **23**, 187 (2004).
[8]D. Townsend, W. Li, S. K. Lee, R. L. Gross, and A. G. Suits, J. Phys. Chem. A **109**, 8661 (2005).
[9]K. C. Lau, Y. Liu, and L. J. Butler, J. Chem. Phys. **123**, 054322 (2005).
[10]D. R. Albert and H. F. Davis, Phys. Chem. Chem. Phys. **15**, 14566 (2013).
[11]J. J. John, M. Brouard, A. Clark, J. Crooks, E. Halford, L. Hill, J. W. L. Lee, A. Nomerotski, R. Pisarczyk, I. Sedgwick, C. S. Slater, R. Turchetta, C. Vallance, E. Wilman, B. Winter, and W. H. Yuen, J. Instrum. **7**, C08001 (2012).
[12]B. Martínez-Haya, I. Zapater, P. Quintana, M. Menéndez, E. Verdasco, J. Santamara, L. Bañares, and F. J. Aoiz, Chem, Phys. Lett. **311**, 159 (1999).
[13]B. Martínez-Haya, P. Quintana, L. Bañares, P. Samartzis, D. J. Smith, and T. N. Kitsopoulos, J. Chem. Phys. **114**, 4450 (2001).
[14]R. A. Morgan, A. J. Orr-Ewing, M. N. R. Ashfold, W. J. Buma, N. P. L. Wales, and C. A. de Lange, J. Chem. Soc. Faraday Trans. **91**, 3339 (1995).
[15]P. Quintana, R. F. Delmdahl, D. H. Parker, B. Martínez-Haya, F. J. Aoiz, L. Bañares, and E. Verdasco, Chem. Phys. Lett. **325**, 146 (2000).
[16]J. Barr, I. Torres, E. Verdasco, L. Bañares, F. J. Aoiz, and B. Martínez-Haya, J. Phys. Chem. A **108**, 7936 (2004).
[17]J.-H. Yoon, K. C. Woo, and S. K. Kim, Phys. Chem. Chem. Phys. **16**, 8949 (2014).
[18]S. Choi, K. W. Choi, S. K. Kim, S. Chung, and S. Lee, J. Phys. Chem. A **110**, 13183 (2006).
[19]S. Nourbakhsh, K. Norwood, H. M. Yin, C. L. Liao, and C. Y. Ng, J. Chem. Phys. **95**, 5014 (1991).
[20]B. Ruscic and J. Berkowitz, J. Chem. Phys. **97**, 1818 (1992).
[21]R. T. Bise, H. Choi, H. B. Pedersen, D. H. Mordaunt, and D. M. Neumark, J. Chem. Phys. **110**, 805 (1999).
[22]J. Berkowitz, G. B. Ellison, and D. Gutman, J. Phys. Chem. **98**, 2744 (1994).
[23]B. Ruscic, J. Phys. Chem. A **119**, 7810 (2015).
[24]*ANL Active Thermochemical Database 1.122* (2018).
[25]B. Ruscic and J. Berkowitz, J. Chem. Phys **98**, 2568 (1993).
[26]R. A. Ingle, C. S. Hansen, E. Elsdon, M. Bain, S. J. King, J. W. L. Lee, M. Brouard, C. Vallance, R. Turchetta, and M. N. R. Ashfold, J. Chem. Phys. **147**, 013914 (2017).
[27]B. Marchetti, T. N. V. Karsili, O. Kelly, P. Kapetanopoulos, and M. N. R. Ashfold, J. Chem. Phys. **142**, 224303 (2015).
[28]A. T. Clark, J. P. Crooks, I. Sedgwick, R. Turchetta, J. W. L. Lee, J. J. John, E. S. Wilman, L. Hill, E. Halford, C. S. Slater, B. Winter, W. H. Yuen, S. H. Gardiner, M. L. Lipciuc, M. Brouard, A. Nomerotski, and C. Vallance, J. Phys. Chem. A **116**, 10897 (2012).
[29]K. Amini, S. Blake, M. Brouard, M. B. Burt, E. Halford, A. Lauer, C. S. Slater, J. W. L. Lee, and C. Vallance, Rev. Sci. Instrum. **86**, 103113 (2015).
[30]G. M. Roberts, J. L. Nixon, J. Lecointre, E. Wrede, and J. R. R. Verlet, Rev. Sci. Instrum. **80**, 053104 (2009).
[31]B. Buijsse, W. J. van der Zande, A. T. J. B. Eppink, D. H. Parker, B. R. Lewis, and S. T. Gibson, J. Chem. Phys. **108**, 7229 (1998).
[32]R. J. Vatsa, C. Majumder, O. D. Jayakumar, S. K. Kulshreshtha, and J. P. Mittal, Proc. Indian Acad. Sci. **113**, 129 (2001).
[33]M. Aschi and F. Grandinetti, J. Chem. Phys. **111**, 6759 (1999).
[34]A. J. Orr-Ewing and R. N. Zare, Annu. Rev. Phys, Chem. **45**, 315 (1994).
[35]D. C. Jacobs and R. N. Zare, J. Chem. Phys. **85**, 5457 (1986).
[36]D. C. Jacobs, R. J. Madix, and R. N. Zare, J. Chem. Phys. **85**, 5469 (1986).
[37]J. M. Nicovich, K. D. Kreutter, C. A. van Dijk, and P. H. Wine, J. Phys. Chem. **96**, 2518 (1992).

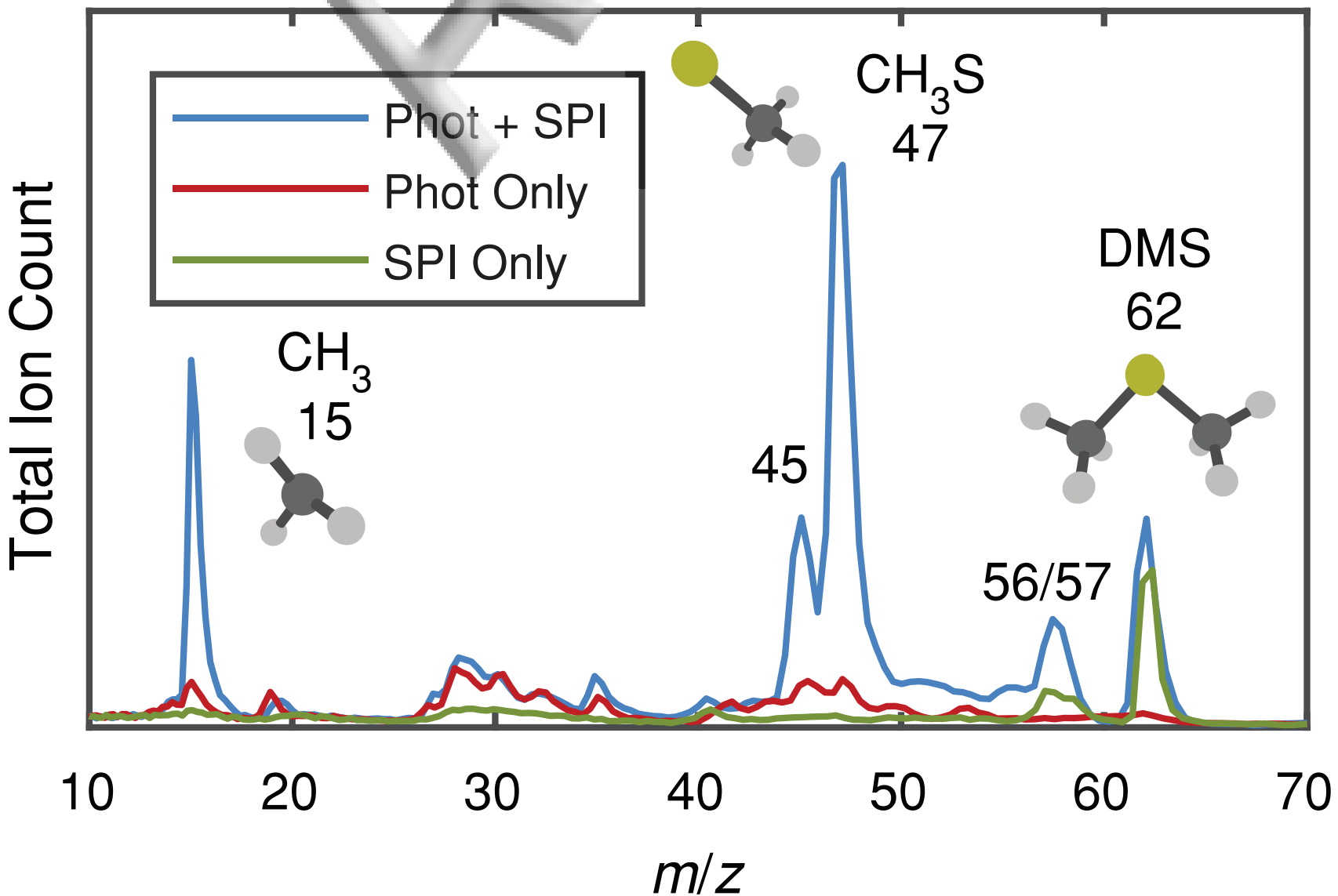
Phot + SPI
Phot Only
SPI Only
Total Ion Count
CH3
15
CH3S
47
45
DMS
62
56/57
10
20
30
40
50
60
70
m/z

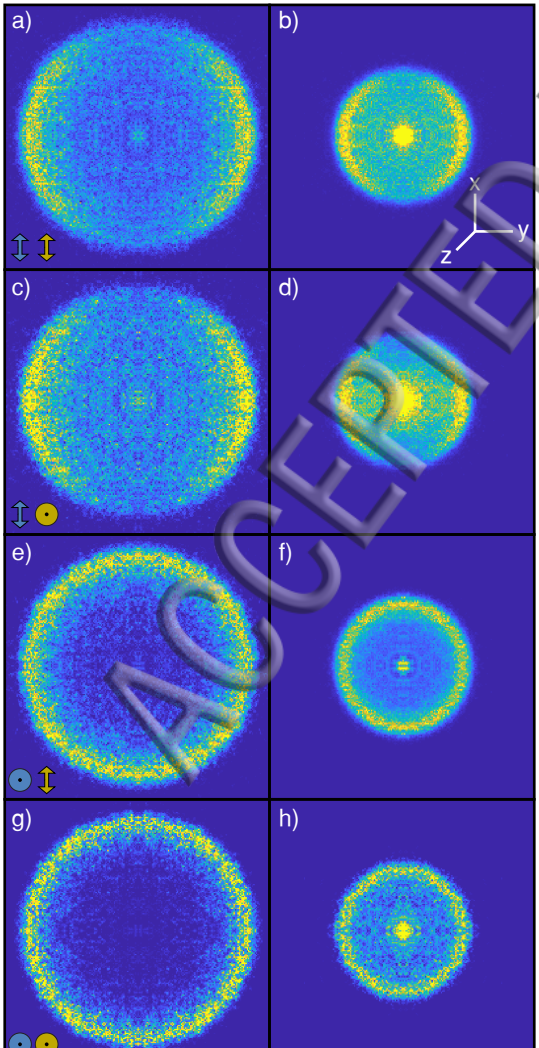

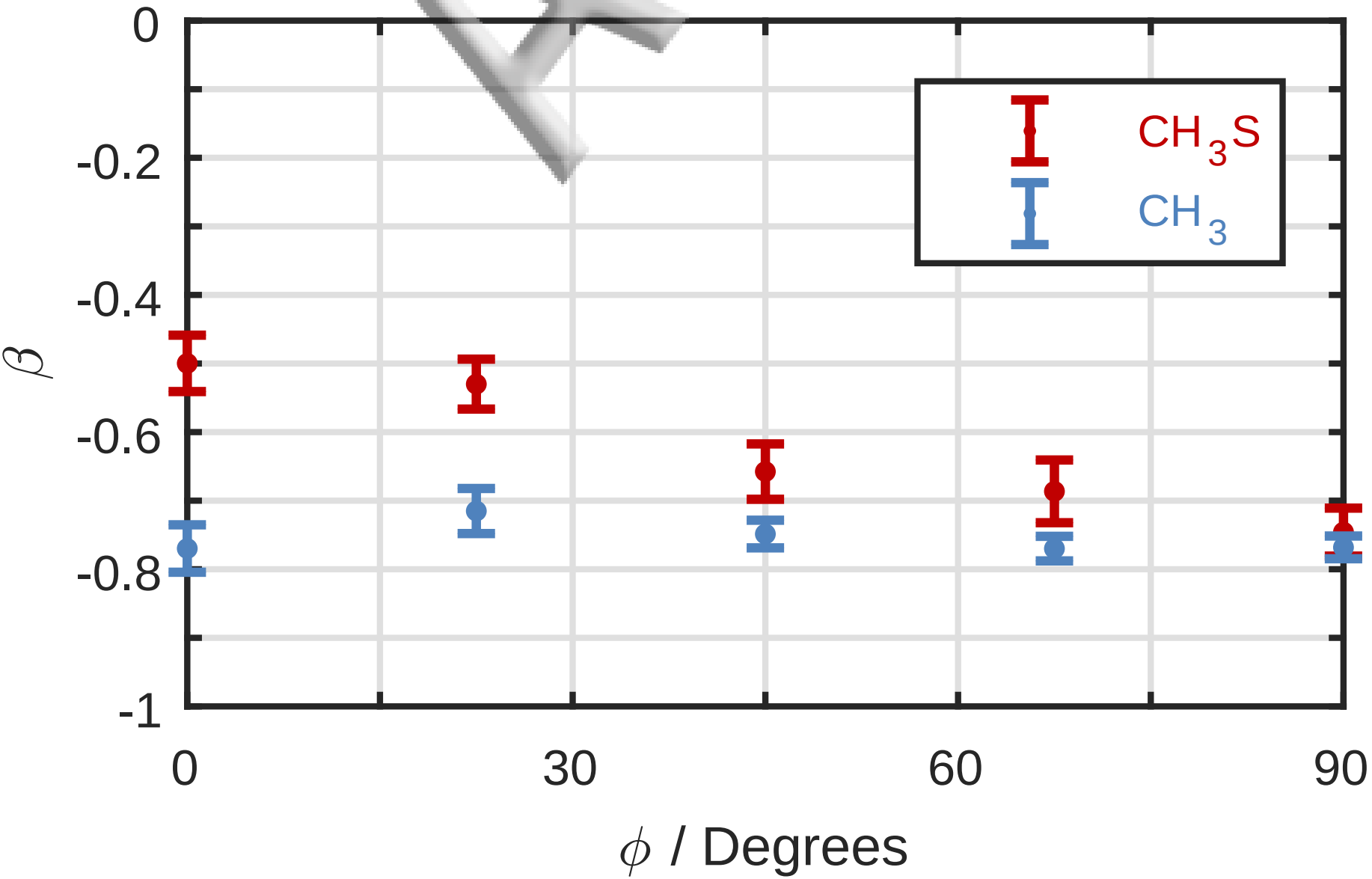
0
-0.2
-0.4
-0.6
-0.8
-1
β
0
30
60
90
ϕ / Degrees
CH3S
CH3

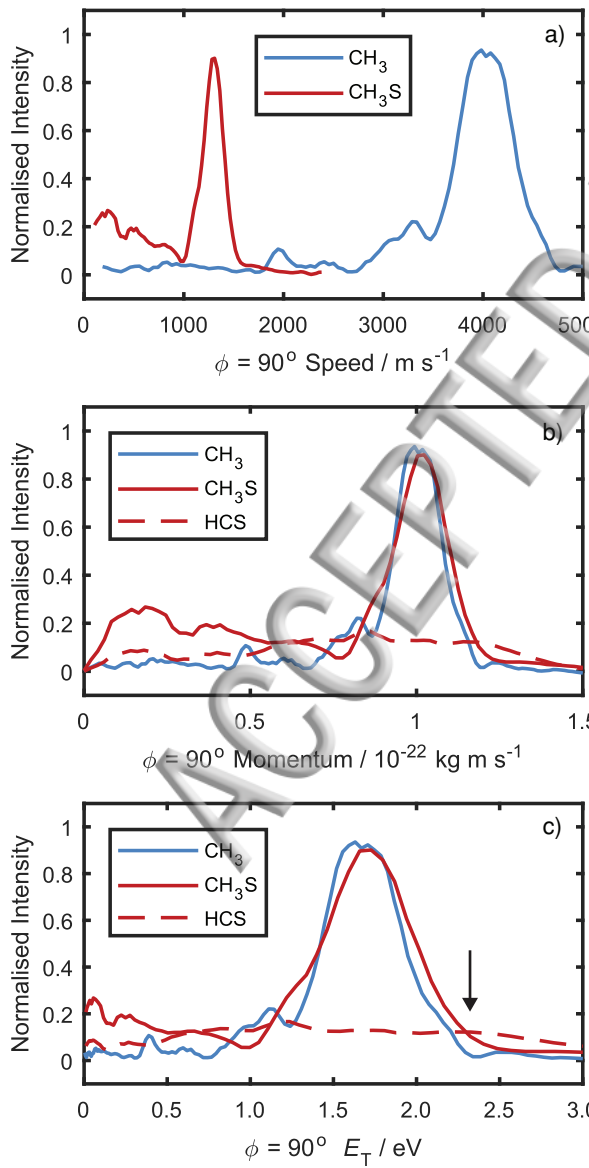
a)
CH3
CH3S
Normalised Intensity
0
0.2
0.4
0.6
0.8
1
0
1000
2000
3000
4000
5000
ϕ = 90° Speed / m s-1
b)
CH3
CH3S
HCS
Normalised Intensity
0
0.2
0.4
0.6
0.8
1
0
0.5
1
1.5
ϕ = 90° Momentum / 10-22 kg m s-1
c)
CH3
CH3S
HCS
Normalised Intensity
0
0.2
0.4
0.6
0.8
1
0
0.5
1.0
1.5
2.0
2.5
3.0
ϕ = 90° ET / eV